Methods and Applications in Fluorescence

TECHNICAL NOTE

Pulse-shaped broadband multiphoton excitation for single-molecule fluorescence detection in the far field

David Nobis, Henry G Sansom and Steven W Magennis

School of Chemistry, University of Glasgow, Joseph Black Building, University Avenue, Glasgow, G12 8QQ, United Kingdom

E-mail: steven.magennis@glasgow.ac.uk

Keywords: pulse shaping, titanium sapphire laser, non-linear excitation, ultrafast lasers

Supplementary material for this article is available online

OPEN ACCESS

RECEIVED
11 June 2022

REVISED
8 November 2022

ACCEPTED FOR PUBLICATION
1 December 2022

PUBLISHED
19 January 2023

Abstract

Multiphoton excitation of fluorescence has many potential advantages over resonant (one-photon) excitation, but the method has not found widespread use for ultrasensitive applications. We recently described an approach to the multiphoton excitation of single molecules that uses a pulse shaper to compress and tailor pulses from an ultrafast broadband laser in order to optimise the brightness and signal-to-background ratio following non-linear excitation. Here we provide a detailed description of the setup and illustrate its use and potential by optimising two-photon fluorescence of a common fluorophore, rhodamine 110, at the single-molecule level. We also show that a DNA oligonucleotide labelled with a fluorescent nucleobase analogue, tC, can be detected using two-photon FCS, whereas one-photon excitation causes rapid photobleaching. The ability to improve the signal-to-background ratio and to reduce the incident power required to attain a given brightness can be applied to the multiphoton excitation of any fluorescent species, from small molecules with low multiphoton cross sections to the brightest nanoparticles.

1. Introduction

In contrast to traditional ensemble methods, single-molecule techniques can reveal information that would otherwise be hidden in the ensemble-averaged signal. Since the first observation of single fluorophores by Orrit and Bernard [1], fluorescence microscopy has developed into one of the key single-molecule tools, in large part because it is non-invasive and can be used *in vivo* [2]. The multiphoton excitation of fluorescent molecules, which involves the quasi-simultaneous absorption of two or more photons, can offer advantages over resonant excitation. For probes, that absorb in the UV region of the electromagnetic spectrum, multiphoton excitation offers a way to use a near-IR excitation source. Multiphoton absorption also affords a deeper penetration of tissue for biological experiments, less out of focus photobleaching of the specimen, less background (due to reduced scattering and resonant absorption) and a better separation of the excitation light from the emission light [3]. The selection rules for multiphoton transitions can also enable alternative excitation pathways [4], while the dynamic range of fluorescence anisotropy measurements is larger [5, 6].

The first observation of the two-photon excitation of single molecules was by Mertz and co-workers; they used two-photon excitation to observe light bursts from freely diffusing rhodamine B molecules [7], with other reports following shortly after [8–11]. Notably, the use of IR light reduced in-focus photobleaching of the fluorophore, which occurred via higher excited states [8, 12]. However, enhanced photobleaching has also been observed in other cases; e.g. via radical formation [13]. In spite of the early promise, there have been relatively few studies that use multiphoton excitation for single-molecule spectroscopy.

A number of obstacles have to be overcome in order to use multiphoton excitation for single-molecule microscopy. The first is the relatively small multiphoton cross section for the typical small organic fluorophores that are used for many single-molecule fluoresence applications. This leads to a low brightness and signal-to-background ratio (SBR). This explains why most applications have been restricted to fluorophores with large multiphoton cross sections such as gold nanoparticles [14], semiconductor nanocrystals [15], highly-conjugated branched organic molecules

[16] or conjugated organic molecules featuring charge or energy transfer [17]. This issue can be partly overcome by the use of a high intensity excitation source. Due to the nonlinearity of the excitation process, the excitation probability has a power of N dependence on the excitation intensity for N-photon absorption. This means that pulsed excitation is the preferred method because it allows very high peak powers. To reduce the average power and minimise photobleaching while maintaining excitation rate, the shortest pulse possible is desirable [18]. While multiphoton excitation is often performed with a tuneable Ti:sapphire laser of *ca.* 150 fs pulse duration, convenient broadband supercontinuum sources are also now widely used [19, 20]. Recently, broadband pulsed lasers with pulsewidths less than 10 fs have become available commercially. However, the use of such lasers leads to another problem, which is the temporal broadening of the pulses due to dispersion by the optical components (particularly the objective lens). It is, therefore, necessary to compensate for this dispersion to ensure that short pulses with high peak power excite the sample.

To achieve this, we built a multiphoton microscope for point excitation that uses active amplitude and phase shaping of ultrafast laser pulses and photon-counting detection. The point excitation allows for future implementation of beam or stage scanning for 2D or 3D imaging. At its heart, the microscope uses a pulse shaper to compress the laser pulses by measuring and compensating for the phase distortion acquired in transit through the optical components. Dantus *et al* first showed that ensemble fluorescence multiphoton microscopy can benefit from such dispersion compensation [21]. More recently, we demonstrated that fluorescent base analogues (FBAs), fluorescent analogues of DNA nucleobases, could be detected down to the single-molecule level with multiphoton excitation [22, 23]. In addition, it was shown previously that two-photon excitation of FBAs can result in less photobleaching than one-photon excitation [24, 25].

In this work, we describe our pulse-shaped broadband multiphoton microscope setup in detail and discuss previously unexplored aspects of the shaping for single-molecule detection. After a short overview of the theory of pulse shaping, we describe the experimental setup followed by a demonstration of the benefits of phase and/or amplitude shaping for single-molecule detection using rhodamine 110 as a model fluorescent dye, and using a DNA oligonucleotide labelled with an FBA. We believe that this approach can be extended to other fluorescent molecules and particles.

2. Theory

Maria Göppert-Mayer calculated the transition rates for multiphoton absorption in her doctoral thesis of 1931, building on Paul Dirac's work on perturbation theory [26]. Two-photon excitation was first demonstrated experimentally in 1961 [27], soon after the invention of the laser. The excitation probablity P_{if}^{N} for the non-resonant, N-photon transition between two states i and f can be determined with 2nd order time-dependent perturbation theory [28]. For an electric field E and transition frequency ω_{if}, P_{if}^{N} can be described as a Fourier component of the power spectrum E^{N} [29]:

$$P_{if}^{N} \propto \left| \int_{-\infty}^{\infty} E^{N}(t) \exp\left(i\omega_{if} t\right) dt \right|^{2}. \tag{1}$$

In the simplified case of a two-level system with a transition frequency ω_{if}, the two-photon excitation probability P_{if}^{2} can be rewritten as [29]:

$$\begin{aligned} P_{if}^{2} &\propto \left| \int_{-\infty}^{\infty} E\left(\frac{\omega_{if}}{2} + \Omega\right) E\left(\frac{\omega_{if}}{2} - \Omega\right) d\Omega \right|^{2} \\ &= \left| \int_{-\infty}^{\infty} \left| E\left(\frac{\omega_{if}}{2} + \Omega\right) \right| \left| E\left(\frac{\omega_{if}}{2} - \Omega\right) \right| \cdot \right. \\ &\left. \exp\left[i\left(\varphi\left(\frac{\omega_{if}}{2} + \Omega\right) + \varphi\left(\frac{\omega_{if}}{2} - \Omega\right) \right) \right] d\Omega \right|^{2} \\ &\equiv A^{(2)}(\omega_{if}) \end{aligned} \tag{2}$$

where $E(\omega)$ and $\varphi(\omega)$ are the spectral amplitude and phase, respectively, Ω is the spectral offset, and $A^{(2)}(\omega_{if})$ is the 2nd order electric field. The implications of equation (2) are illustrated in figure 1, showing that photons of different frequencies can be combined to bridge the energy gap, provided they are in phase. The same approach can be extended to higher-order multiphoton processes.

For a molecule with a broader absorption spectrum than a two-level system, the absorption probability can be expressed by [30]:

$$P^{2} \propto \int_{-\infty}^{\infty} g^{2}(\omega) A^{(2)}(\omega) d\omega \tag{3}$$

where $g^{2}(\omega)$ is the non-linear excitation spectrum. Similar equations can be derived for the nth order electric field $A^{(n)}(\omega_{if})$ for higher-order processes [30].

Equations (2) and (3) show that the excitation probability can be influenced by manipulation of $E(\omega)$ and $\varphi(\omega)$. A maximum excitation efficiency is achieved for a broad laser spectrum when the phase is constant (*i.e.* the pulse is transform-limited), or over a narrower spectral range with a phase that is point symmetric around ω_{if}.

If a short light pulse travels through optical components (e.g. lenses) the phase function is altered due to dispersion. As can be seen from equation (2), this will affect the non-linear absorption efficiency. To understand the impact an added phase has on the pulse, it is useful to look at the Taylor expansion of the phase function:

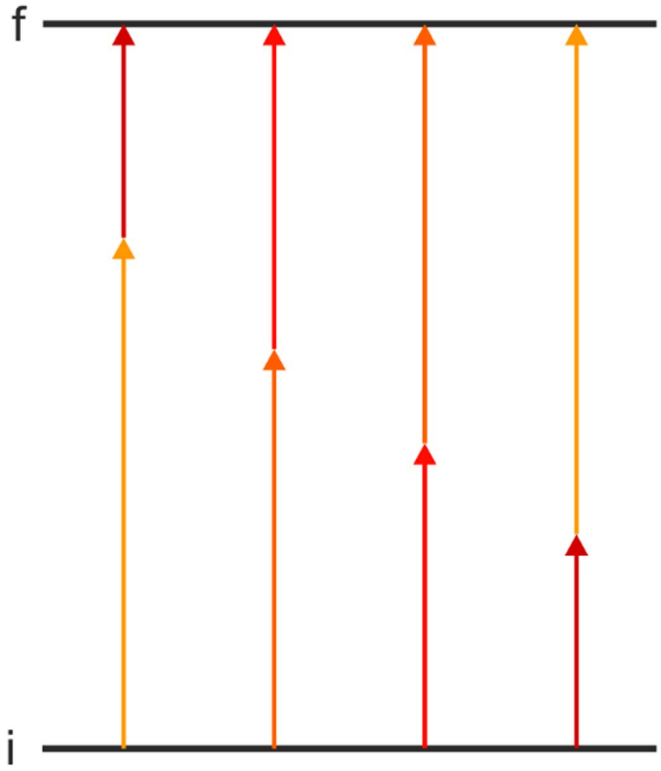

Figure 1. Two-photon excitation of a two-level system showing that combinations of different photons can be used to excite the system.

$$\varphi(\omega) = \varphi(\omega_0) + \varphi''(\omega_0)(\omega - \omega_0) + \frac{1}{2}\varphi''(\omega_0)(\omega - \omega_0)^2 + \frac{1}{6}\varphi'''(\omega_0)(\omega - \omega_0)^3 \ldots \quad (4)$$

Each of the components of this expansion has a different influence on the pulse: the zeroth-order term accounts for the absolute phase in the time domain, the first-order term for a time shift of the envelope fuction, the second-order term (group delay dispersion, GDD) for a linear chirp and the third-order term for an assymmetric pulse shape [31, [32].

In order to compensate for the phase distortion that is added to the excitation pulse by the setup, the phase has to first be measured. There are many approaches to measuring the phase of an ultrafast pulse [33]. Due to the shortness of the pulses, it is not possible to shape them in the time domain. Instead, the shaping takes place in the frequency domain. A very common method is the 4 f setup. It uses a grating that diffracts the incoming light beam into its spectral components. One focal length away, a lens focuses each spectral component into the Fourier plane. This Fourier plane represents the Fourier transformation of the initial laser pulse in its spatial dimensions. In this plane, an active medium can be used to shape the pulse in the frequency domain. One further focal length after the Fourier plane, an additional lens or mirror focuses the beam onto a second grating which recombines the spectral components into one beam. Many different active media and versions of the 4 f setup have been developed [33].

In this work, we use the Multiphoton Intrapulse Interference Phase Scan (MIIPS) method in combination with the Chirp Reversal Technique (CRT). MIIPS was developed by the Dantus group [30, 34–37] and CRT by Loriot and co-workers [38]. These methods work by recording the output of a thin second harmonic generation (SHG) crystal while the pulse shaper applies a range of known phase functions to the pulse. The SHG signal is proportional to $A^{(2)}(\omega_{if})$ and thus allows retrieval of the unknown phase distortion in the setup. MIIPS commonly uses sinusoidal reference functions. By neglecting terms higher than second order in equation (4), the SHG signal in MIIPS is maximised when the second-order dispersion is cancelled. Once this phase is known, it is straightforward to apply a compensation phase mask to the pulse shaper. After compensation, this process can be repeated to cancel higher-order dispersion and achieve compressed pulses at the location of the sample. The CRT method applies quadratic phase functions to measure the second-order dispersion of the setup, and complements MIIPS because it is good at correcting large second order variations in phase. Details of MIIPS and CRT can be found in the references above; both methods are implemented here using commercially available software (see below for details).

3. Methodology

3.1. Setup

3.1.1. Excitation

A schematic of the multiphoton setup is shown in figure 2 [39]. The light is generated by a pulsed broadband Ti:

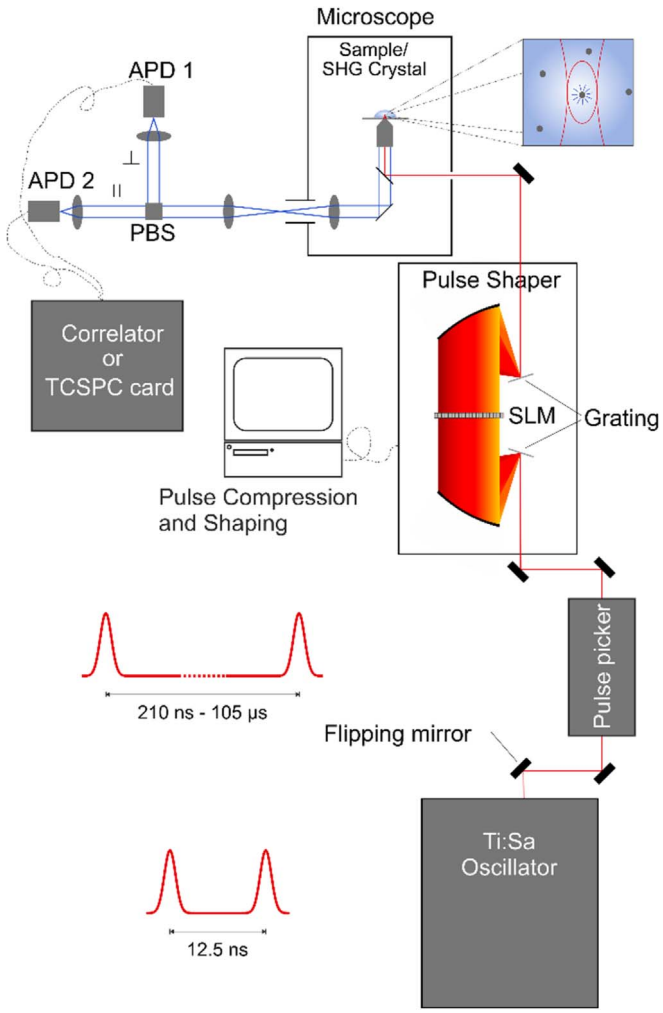

Figure 2. Schematic of the multiphoton setup. The red line depicts the excitation light and the blue line depicts the emitted light. For details see text.

sapphire laser (Coherent, Vitara UBB). It has a tuneable spectral width of <180 nm to >220 nm (at −10 dB), 10 fs pulse width at the output (at maximal bandwidth) and 80 MHz repetition rate. The average output power measured for the laser's ultra-broadband setting (used throughout this work) was 400 mW. If necessary, the repetition rate of the laser can be reduced to between 9.5 kHz and 4.75 MHz by adding a pulse picker (Coherent, Model 9200 Pulse Picker) into the beam path by a flipping mirror (the schematic in figure 2 shows the operation with the pulse picker though this was not used in this work). To adjust the beam width to a value suitable for the pulse picker and the pulse shaper, a 2× reducing telescope and a 2.5× expanding telescope are placed before and after the pulse picker, respectively (not shown in figure 2). The reducing telescope consists of a convex (R = 200 mm) and a concave (R = 400 mm) mirror (both with custom dielectric coating, provided by Coherent), the expanding telescope consists of a convex (R = 250 mm) and a concave (R = 100 mm) mirror (Eksma Optics, 092-0125R-250 and 092-0225 R + 100, respectively). All mirrors are protected silver mirrors by Thorlabs (PF10-03-P01), except for those in the reducing telescope (see above).

After the laser/pulse picker, the beam passes through a cover slip, which reflects part of the beam onto a photodiode (Becker and Hickl, PDM-400) to generate a reference signal for the photon counting (see below). The beam then enters the pulse shaper (Biophotonics, MIIPS-Box 640). The pulse shaper uses a liquid crystal spatial light modulator (LC-SLM) from Jenoptik (SLM-S640) for pulse shaping. It consists of two 640 pixel-wide LC-SLM in series. It can add a maximum phaseshift of 2π (at 1500 nm) to 7π (at 430 nm). To enable amplitude shaping in addition to phase shaping, a polarizer (Moxtek, wiregrid UBB02A) is mounted in front of the LC-SLM stack. The pulse shaper is controlled by the MIIPS software 2.0 (Biophotonic Solutions Inc.), which also implements the MIIPS/CRT scan. In our setup, the throughput of the shaper was determined to be 30% of the incoming laser power.

After the pulse shaper, the beam passes through a longpass filter with a cut-off wavelength of 655 nm (Chroma, ET665lp). This removes spectral components

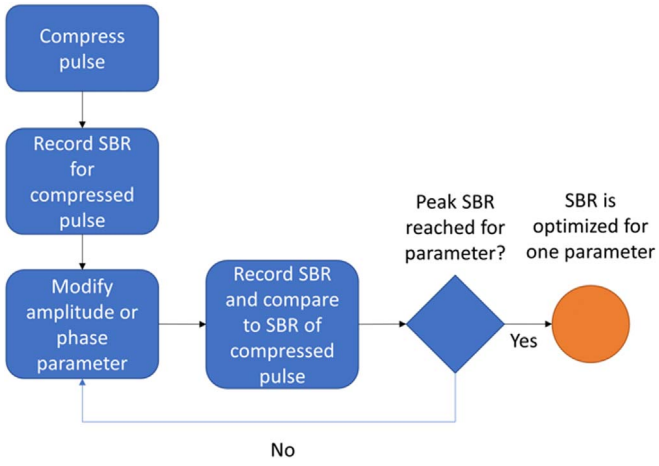

Figure 3. Optimisation of SBR. After compressing the pulse, the SBR is recorded and is used as a reference for subsequent measurements with altered pulse shapes.

that are not filtered post excitation. Subsequently the beam is guided into an inverted microscope (Olympus, IX71). Here the light is reflected into the objective by a dichroic mirror (Chroma, 675dcspxr). The light is focussed onto the sample by a 60×, water immersion objective with a NA of 1.2 (Olympus, UPlanSApo 60×). The sample is placed on a borosilicate glass coverslip (Thermo Scientific, Menzel Gläser, #1.5, thickness 0.16–0.19 mm). For temperature control of the sample, an incubator (Live Cell Instrument, LCI CU-501) can be fitted to the microscope stage.

3.1.2. Detection

The emitted light is collected by the objective, transmitted through the dichroic mirror and exits the microscope through the right-hand side port. The emitted light is filtered (Semrock, FF01-650/SP) and collimated by a plano-convex lens, before it passes through a polarising beam splitter (Qioptiq, G335564000), which splits the fluorescence light into its parallel and perpendicular polarised components (relative to the plane of polarisation of the excitation beam). Each beam is then focussed down onto a 50 μm SPAD (Micro Photon Devices, MPD PDM 50c and MPD $PD-050-CTB); all lenses are from Edmund Optics (PCX with coating UV–vis CTD TS). The SPADs are Peltier-cooled silicon diodes, with an active quenching circuit. They have a detection efficiency of $>$ 45% at 550 nm, a timing resolution of $<$250 ps, a dead time of 77 ns and a dark count rate of $<$0.1 kHz. A 1″ lens tube system (Thorlabs) is used to enclose the detection unit, which makes the setup flexible for additional detectors in the future (e.g. channels for different colours).

The TTL signal from the SPADs passes through a router (Becker and Hickl, HRT 82) to add the identity of the channel to the signal, which is then recorded with a time-correlated single-photon counting (TCSPC) card (Becker and Hickl, SPC-130). The signal is recorded in the 'reverse start stop' TCSPC configuration [40, 41]. Each photon event is stored with its micro time (time to the next laser pulse) and its macro time (time from the beginning of the experiment). This allows the real-time display of multi-channel scaling (MCS) traces and the post-acquisition analysis via fluorescence correlation spectroscopy (FCS) and photo-counting histograms (PCH).

As an alternative to the photon-counting approach, all FCS measurements in this study were recorded with a hardware correlator (ALV-GmbH, ALV-7002) and were fitted to a model of diffusion through a 3D Gaussian volume (equation (5)), taking the background contribution I_B and the strength of the signal S into account [8]:

$$G(t) = \frac{(1 - I_B/S)^2}{\sqrt{8}\,N} \times \left(\frac{1}{1 + (t/\tau_D)}\right) \cdot \sqrt{\frac{1}{1 + (w_0/z_0)^2 (t/\tau_D)}} \quad (5)$$

where w_0 and z_0 are the waist and the height of the excitation volume and τ_D is the average diffusion time.

3.2. Optimisation and measurement

The process for pulse optimisation is illustrated in figure 3. Details of the pulse compression are given in the SI. After compressing the pulse, the SBR for fluorescence is recorded as a benchmark for later modifications, where the SBR is the ratio of the mean signal (minus the mean background) to the mean background. Changes can be made to the pulse amplitude or phase followed by new measurements of the SBR to compare with that of the compressed pulse. As a starting point for the optimization, usually a function was chosen that leads to a peak of $A^{(2)}(\omega)$ in the vicinity of twice the one-photon peak absorption. For the optimization described in section 4, the peak position and the width of the peak were varied.

To avoid evaporation, short (10 s) illumination times were used and the laser was blocked in between optimisation measurements. After each measurement, the SBR for the compressed pulse was compared with the newly optimised pulse. For long sample measurements, evaporation was reduced by placing the sample in an incubator (22 °C).

3.3. One-photon excitation

For one-photon excitation, the same microscope (section 3.1) was used, with excitation from a 405 nm CW laser (Hübner Photonics, Cobolt 06-MLD). The dichroic was a 412 nm longpass filter (Chroma, T412lpxt-UF1). The emission was collected through a 565/133 nm bandpass filter (Semrock, FF01-565/133). A 100 μm pinhole was inserted in the emission path for confocal detection.

3.4. Sample preparation

In order to reduce the background to a tolerable level, all tubes, pipette tips and coverslips were cleaned before they came in contact with the sample. The established cleaning protocol was rinsing with HPLC grade methanol and ultra-pure water, and drying with N_2.

The stock solution of rhodamine 110 (Fluka 83695) was prepared by dissolving it in ultrapure water (Direct Q3, Merck Millipore) at a concentration of 1 mM. The concentration was checked by UV–vis spectroscopy. To obtain samples for the measurements, the stock solution was diluted down with ultrapure water in several steps to the desired concentration.

For the SBR experiments with the sinusoidal phase shape, Tris buffer was used to dilute the sample from the stock solution. The buffer was prepared by dissolving Tris (Trizma base, BioUltra, Sigma-Aldrich) at 20 mM and NaCl (analytical reagent grade, Fluka) at 150 mM in ultrapure water. To adjust the pH to 7.8, HCl solution (Sigma-Aldrich) was added in a second step.

The DNA oligonuclotide incorporating the nucleobase analogue tC, with sequence 5' AAT CTC AC**tC** AGC TGA TCA CAT TGC TA, was synthesised (Purimex GmbH, Grebenstein) using the tC-CE phosphoramidite (Glen Research). The measurement buffer contained 20 mM Tris and 150 mM NaCl at pH 7.5; the buffer was filtered with activated charcoal before use.

4. Results and discussion

To demonstrate the effect of pulse shaping on single-molecule fluorescence measurements, we present measurements of solutions of rhodamine 110 in ultrapure water. First we show the effect that pulse compression to the transform limit has on the SBR and on single-molecule brightness. We then explore what effect other pulse shapes can have on the SBR. We then extend this approach to detect the fluorescence from single-stranded DNA that has been labelled with a FBA, showing the benefit of our multiphoton approach in comparison to one-photon excitation.

4.1. Pulse compression

The pulses were compressed by the method described above. The compression algorithm converges after 6–8 steps. The resulting phase function is shown in figure 4(A) (dashed line). The compression leads to a shortening of the pulse from several 100 fs to only 7.5 fs. This value was calculated via fast Fourier transform (FFT) using the measured spectrum and the average remaining phase as an input. This result is very close to the calculated transform-limited pulse, which is 7 fs long. Due to the compression, the peak intensity increases by a factor of 82. The FFTs for the uncompressed and compressed pulses are shown in figure 4(B). The pulse compression leads to a significant increase in peak irradiance. The maximum pulse energy that is accessible after the objective is 1.07 nJ at 80 MHz. This value leads to a maximum accessible average irradiance in the focus of the beam of 24.98 TW cm^{-2}. In comparison, the maximum accessible peak irradiance of the uncompressed pulse is 0.30 TW cm^{-2}. This value is smaller than the lowest irradiance used with compressed pulses (which was 0.45 TW cm^{-2} at 1.54 mW), even though the average power is 50 times as high.

In order to analyse the consistency of the algorithm, 9 further MIIPS steps were carried out and the average remaining phase is shown in figure 4(C). The error bars depict the variance of these 9 scans. It can be seen that the phase is almost constant between 700 nm and 900 nm. For values lower than 700 nm, the uncertainty increases, which can be attributed to the fact that the SHG spectrum only extends down to 350 nm. However, since the spectral intensity of the laser is low in this wavelength region, the influence on the overall compression should also be low (see SI and Supplementary figure 1 for further details on the reproducibility of the pulse shaping).

Further evidence that the compression process works well comes from the comparison of the calculated and measured SHG spectra (figure 4(D)). The calculation was done according to equation (2). After normalisation to the respective maximum, the two curves align well qualitatively and differences can be attributed to the diminishing phase matching at the edges of the spectrum.

Next, the effect of pulse compression was investigated with a 10 nM rhodamine 110 solution. The dependence of the emission on the excitation power (power series) is shown in figure 5(A) (see Supplementary figure 2 for log-log plots). The emission after the excitation with a compressed pulse is compared to the

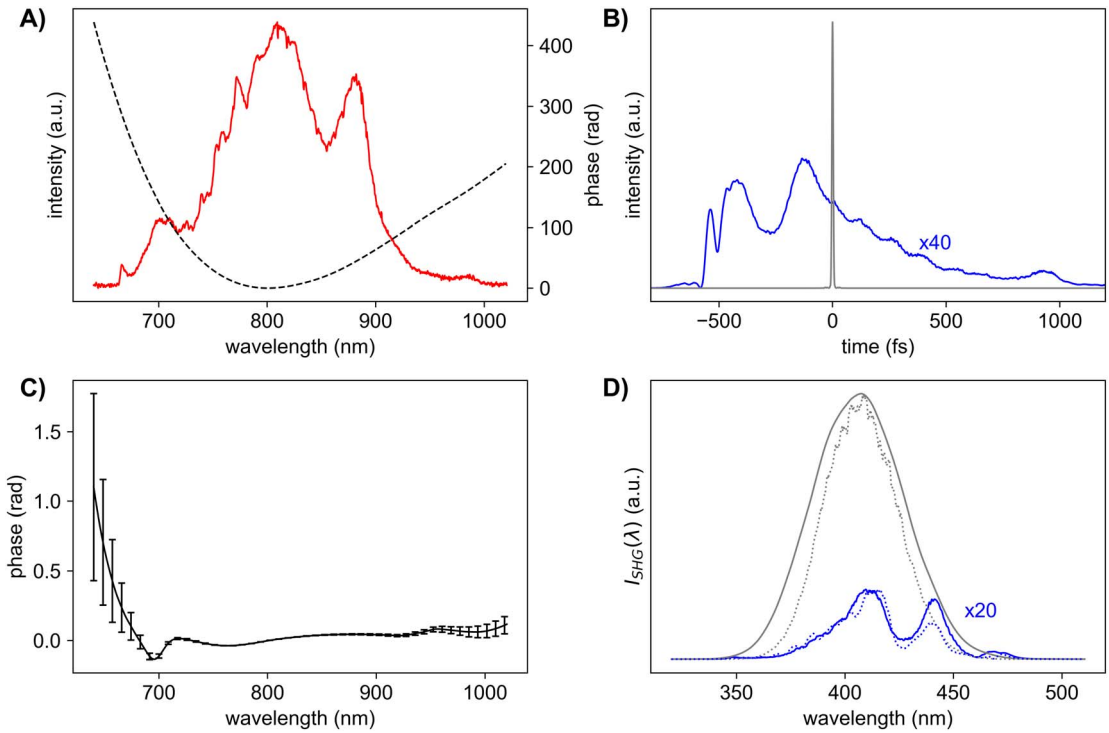

Figure 4. (A) The spectrum of the excitation light is shown in red and the spectral phase (measured with the MIIPS/CRT method) is shown in black (dashed line). (B) The shape of the pulse in the time domain before compression (blue) and after compression (black). (C) The residual phase after 8 MIIPS/CRT iterations. The mean residual phase of a further 9 scans performed after the initial 8 scans is shown. The error bars depict the variance of those 9 scans. (D) The intensity of the SHG signal before (blue lines) and after compression (black lines). The measured values (dotted lines) are compared to the calculated values (solid lines). The maxima of the measured curves were normalised to the maxima of the calculated curves.

emission after excitation with an uncompressed pulse. It can be seen that after compression a much higher emission count rate is reached at lower excitation powers. To determine the point where saturation starts, power law functions were fitted to the power series (Supplementary figure 2). The onset of saturation was assumed to be at the first point that would lead to an exponent smaller than 2. This analysis shows that the last measurements before saturation occurs after excitation with a power of 5.9 mW for the compressed pulses and 19.9 mW for the uncompressed pulses. The count rate at these points was 20.9 kHz and 10.7 kHz, respectively. Therefore, compression leads to a 2-fold increase in (unsaturated) count rate at only a quarter of the power.

In the next step we analysed the SBR. This was done by comparing the emission count rate from the sample with that from pure water. The result for compressed and uncompressed pulses at different excitation powers is shown in figure 5(B). The maximum SBR increased by a factor of 2.1 through compression (from 110 to 234) at a fifth of the average power. For the highest count rate before saturation, the SBR increased by a factor of 2.4.

In order to investigate the effect of compression on single-molecule measurements, MCS traces were recorded for a rhodamine 110 solution at a concentration of 1 pM. The obtained counts over time can be found in figure 5(C). The integration time per datapoint was 1 ms. The figure shows traces obtained from pure water (background) and from the sample (signal). Signal and background are shown for both compressed and uncompressed pulses. For both cases, the power that leads to the highest SBR was used (40.2 mW for the uncompressed pulses and 12.9 mW for the compressed pulses). It is clear that compression leads to much higher count rates for the sample, while not increasing the background noticeably, even though the average power was decreased by a factor of more than 3 (figure 5(C)).

To quantify these results, a PCH analysis was performed (figure 5(D)). Here, each bar shows the frequency at which a certain count rate occurs in figure 5(C). It can be seen that the probability for a clear single-molecule event to appear in the trace increases greatly upon compression. It is 1.3×10^{-5} before compression and 3.4×10^{-5} after compression (calculated by summing all probabilities after the last appearance of the background in the PCH). In addition, the average number of counts for such an event almost doubled (from 6 to 10 counts).

4.2. Sinusoidal phase

We have shown recently that shaping the amplitude of a compressed pulse, by altering the centre and width of the laser spectrum, could significantly increase the SBR [22, 24]. Here we explore the effect on $A^{(2)}(\omega_{if})$ of

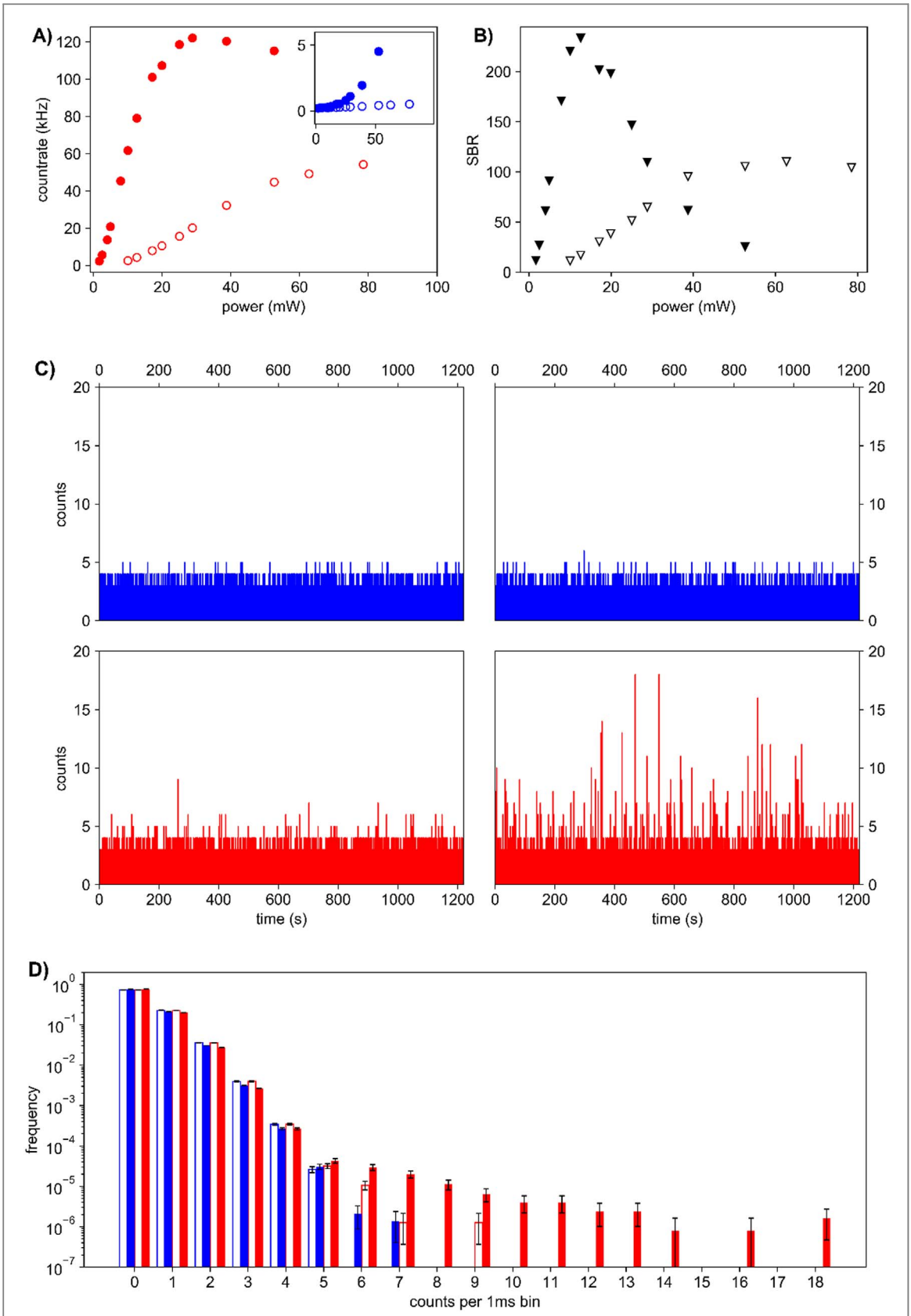

Figure 5. Comparison of the signal from a dilute rhodamine 110 solution, before and after compression. A) power series from rhodamine 110 before compression (red open circles) and after compression (red filled circles). The inset shows the same for pure water (open and filled circles for before and after compression, respectively). The concentration was 10 nM B) SBR before (open triangles) and after compression (filled triangles). C) Comparison of the MCS traces from pure water (blue, top) and 1 pm rhodamine 110 in water (red, bottom). The left two panels show data without pulse compression and the right two panels show data with pulse compression. The excitation power that leads to the best SBR was chosen for each measurement (40 mW uncompressed, 12.9 mW compressed; 1 ms time bins). D) The PCH from the data shown in C). Blue shows data from pure water, red from rhodamine 110; empty bars are before and filled bars after compression.

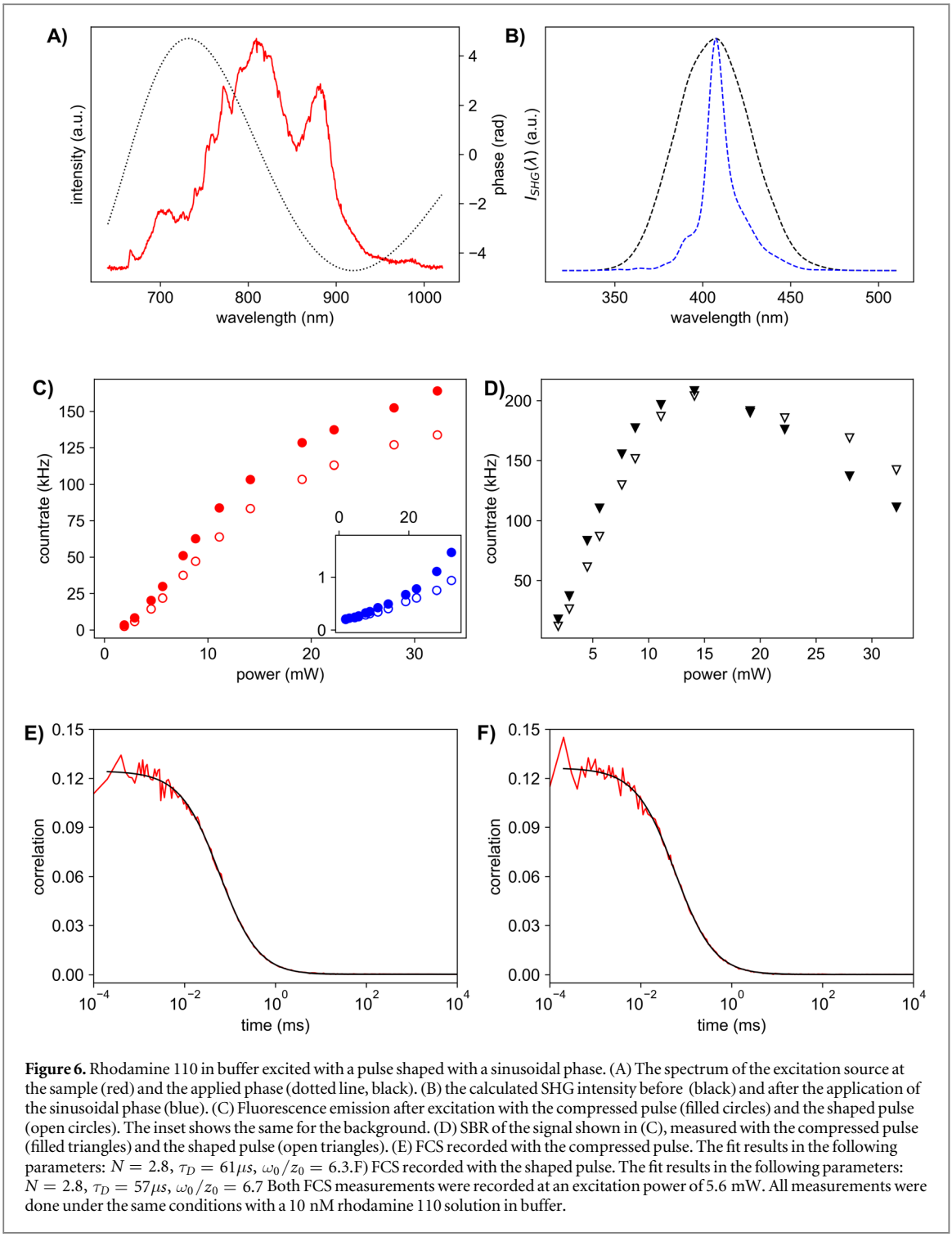

Figure 6. Rhodamine 110 in buffer excited with a pulse shaped with a sinusoidal phase. (A) The spectrum of the excitation source at the sample (red) and the applied phase (dotted line, black). (B) the calculated SHG intensity before (black) and after the application of the sinusoidal phase (blue). (C) Fluorescence emission after excitation with the compressed pulse (filled circles) and the shaped pulse (open circles). The inset shows the same for the background. (D) SBR of the signal shown in (C), measured with the compressed pulse (filled triangles) and the shaped pulse (open triangles). (E) FCS recorded with the compressed pulse. The fit results in the following parameters: $N = 2.8$, $\tau_D = 61\mu s$, $\omega_0/z_0 = 6.3$.F) FCS recorded with the shaped pulse. The fit results in the following parameters: $N = 2.8$, $\tau_D = 57\mu s$, $\omega_0/z_0 = 6.7$ Both FCS measurements were recorded at an excitation power of 5.6 mW. All measurements were done under the same conditions with a 10 nM rhodamine 110 solution in buffer.

altering the phase of a compressed pulse, and its potential use insingle-molecule fluorescnce detection.

A sinusoidal phase was applied to the spectrum (see figure 6(A)):

$$\varphi(\omega) = \alpha \sin(\gamma(\omega - \omega_0)) \tag{6}$$

with $\alpha = 1.5\pi$ and $\gamma = 6$ fs. A sinusoidal function was chosen because it is an easy-to-parametrise point-symmetric function [42]. The point symmetry leads to an excitation probability as good as the compressed pulse for a very narrow energy range (cf equation (2)). This could be useful to tune the excitation phase so that it only excites the sample but not impurities. Similar approaches have been used for selective excitation in ensemble two-photon microscopy *in vivo* [43]. To demonstrate the effect of a sinusoidal phase, figure 6(B) shows the calculated SHG intensity before and after application of the sinusoidal phase.

To find the optimal phase shape for a rhodamine 110 solution, ω_0 was varied while recording the emission count rate. The optimal phase was found to be centred around 815 nm (shown in figures 6(A) and

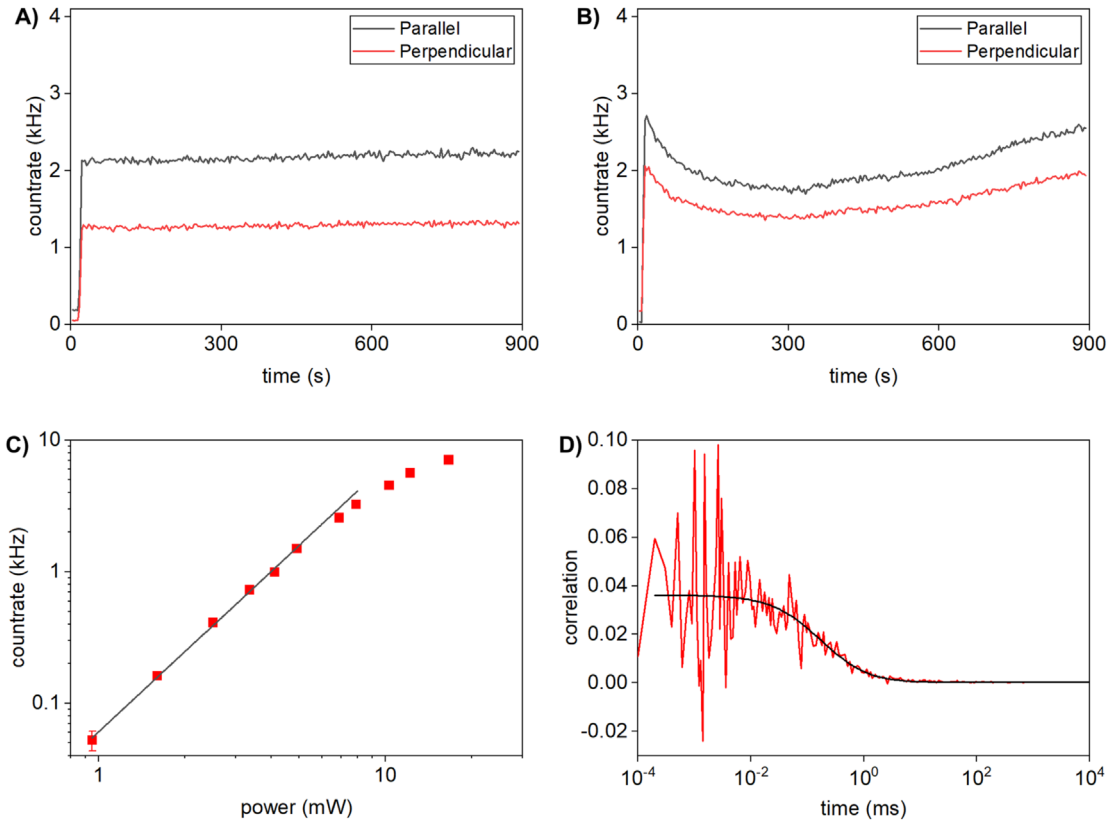

Figure 7. Comparison of the photostability of an oligonucleotide containing tC under one and two-photon excitation. The concentration was 40 nM for all measurements. (**A**) Stable count rate traces from non-resonant excitation at 800 nm (two-photon). The excitation power was 10.5 mW; the laser was blocked for the first ca. 30 s of the measurement. (**B**) Count rate traces from resonant excitation at 405 nm (one-photon) showing significant photobleaching before recovery. The excitation power was 5 μW; the laser was blocked for the first ca. 30 s of the measurement. The buffer produced a constant background signal of 0.25 kHz. (**C**) Two-photon power series measurements. The gradient of the linear region is 2.03 indicating a two-photon process. No higher-order behaviour was observed. The onset of saturation is around 7 mW. (**D**) FCS after two-photon excitation. From the fit (black line), the average number of molecules in the focus is 12.6 ± 1.8, the diffusion time is 226 ± 25 μs and the count rate per molecule is 0.34 ± 0.03 kHz.

(B)). Adding this phase to the compressed pulse leads to a drop in the peak intensity of the laser pulse in the time domain by a factor of 0.4.

As can be seen in figure 6(C), the addition of the sinusoidal phase function only leads to a slight drop in the signal intensity. Furthermore, the SBR stays essentially the same after adding the phase to the excitation pulses (208 before adding the phase and 204 after the sinusoidal was added, see figure 6(D)). To make sure that the observed effect is not occurring due to a change of the observation volume, fluorescence correlation spectroscopy (FCS) measurements were carried out (see figures 6(E) and (F)). Fits to the obtained curves show that in both cases the average number of molecules in the excitation volume was 2.8. This leads to a count rate per molecule (CPM) of 11.6 kHz in the case of the compressed pulse and 9.1 kHz with the added sinusoidal phase. This shows that it is possible to have selective excitation, with a substantial reduction in laser pulse peak intensity, without compromising on SBR and, to a lesser extent, overall brightness.

4.3. Multiphoton detection of a DNA oligonucleotide labelled with a fluorescent nucleobase analogue

As a demonstration of the benefit of pulse-shaped multiphoton excitation, we studied a DNA oligonucleotide that incorporated an FBA, 1,3-diaza-2-oxophenothiazine (tC) [44, 45]. We showed previously that a different single-stranded DNA containing tC was more stable under two-photon excitation than one-photon excitation but that the two-photon brightness was insufficient to obtain an FCS curve [25]. Using the pulse-shaped microscope described here, we measured a tC-labelled oligonucleotide inTris buffer. We also performed the same measurement with one-photon excitation, where the only difference in the setup was the replacement of the broadband laser with a 405 nm CW laser, the addition of a pinhole (for confocality) and a change in the microscope's dichroic and barrier filters (figure 7).

Excitation with the transform-limited output of the broadband Ti:sapphire laser resulted in stable tC

emission (figure 7(A)). In contrast, excitation of the same solution at 405 nm with a power that gave similar emission intensities to the two-photon experiment, led to rapid bleaching of the tC followed by a longer recovery due to diffusion of fresh molecules into the excitation volume (figure 7(B)). The background due to the buffer was constant under the same conditions at around 0.25 kHz. Varying the power of the IR laser confirmed that tC is excited via a two-photon process (figure 7(C)). After shaping, the tC was bright enough to record an FCS curve (figure 7(D)). This highlights the potential benefits that can be gained using pulse-shaped multiphoton excitation.

5. Conclusion

We have presented a home-built single-molecule setup that uses pulse-shaped multiphoton excitation for single-molecule fluorescence detection. It uses the measurement of the spectral phase at the focus of the laser and the subsequent compensation of this phase to maximise the peak intensity of the excitation light source. The pulse shaper also enables further optimisation through deliberate manipulation of amplitude and/or phase. We also demonstrated the potential of further phase shaping of the compressed pulses, showing that it is possible to achieve selective excitation at reduced peak intensity while maintaining a high SBR and brightness. The multiphoton approach described here could be beneficial for applications in biological samples, where high peak intensity might cause damage to cells and tissue. Furthermore, it is also possible to extend this approach to other imaging modalities such as total internal reflection fluorescence (TIRF) [46], and it should be applicable to emerging super-resolution methods [47].

Acknowledgments

We thank Dmitry Pestov (IPG Photonics) for invaluable assistance in implementing the pulse shaping. We gratefully acknowledge the support of the EPSRC for funding studentships (DN and HS). The authors have declared that no conflicting interests exist.

Data availability statement

All data that support the findings of this study are included within the article (and any supplementary files).

ORCID iDs

Henry G Sansom https://orcid.org/0000-0002-4893-8511
Steven W Magennis https://orcid.org/0000-0002-4327-8366

References

[1] Orrit M and Bernard J 1990 Single pentacene molecules detected by fluorescence excitation in a p-terphenyl crystal *Phys. Rev. Lett.* **65** 2716–9
[2] Hell S W 2007 Far-field optical nanoscopy *Sci.* **316** 1153–8
[3] He G S, Tan L S, Zheng Q and Prasad P N 2008 Multiphoton absorbing materials: molecular designs, characterizations, and applications *Chem. Rev.* **108** 1245–330
[4] Makarov N S, Drobizhev M, Wicks G, Makarova E A, Lukyanets E A and Rebane A 2013 Alternative selection rules for one- and two-photon transitions in tribenzotetraazachlorin: quasi-centrosymmetrical pi-conjugation pathway of formally non-centrosymmetrical molecule *J. Chem. Phys.* **138** 8
[5] Gryczynski I, Malak H and Lakowicz J 1995 Three-photon induced fluorescence of 2,5-diphenyloxazole with a femtosecond Ti:sapphire laser *Chem. Phys. Lett.* **245** 30–5
[6] Birch D J S 2001 Multiphoton excited fluorescence spectroscopy of biomolecular systems *Spectrochim. Acta A* **57** 2313–36
[7] Mertz J, Xu C and Webb W W 1995 Single-molecule detection by two-photon-excited fluorescence *Opt. Lett.* **20** 2532–4
[8] Brand L, Eggeling C, Zander C, Drexhage K H and Seidel C A M 1997 Single-molecule identification of Coumarin-120 by time-resolved fluorescence detection: Comparison of one- and two-photon excitation in solution *J. Phys. Chem. A* **101** 4313–21
[9] Plakhotnik T, Walser D, Pirotta M, Renn A and Wild U P 1996 Nonlinear spectroscopy on a single quantum system: two-photon absorption of a single molecule *Sci.* **271** 1703–5
[10] Sanchez E J, Novotny L, Holtom G R and Xie X S 1997 Room-temperature fluorescence imaging and spectroscopy of single molecules by two-photon excitation *J. Phys. Chem. A* **101** 7019–23
[11] Lewis M K, Wolanin P, Gafni A and Steel D G 1998 Near-field scanning optical microscopy of single molecules by femtosecond two-photon excitation *Opt. Lett.* **23** 1111–3
[12] Eggeling C, Widengren J, Rigler R and Seidel C A M 1998 Photobleaching of fluorescent dyes under conditions used for single-molecule detection: Evidence of two-step photolysis *Anal. Chem.* **70** 2651–9
[13] Dittrich P S and Schwille P 2001 Photobleaching and stabilization of fluorophores used for single-molecule analysis with one- and two-photon excitation *Appl. Phys. B* **73** 829–37
[14] Olesiak-Banska J, Waszkielewicz M, Obstarczyk P and Samoc M 2019 Two-photon absorption and photoluminescence of colloidal gold nanoparticles and nanoclusters *Chem. Soc. Rev.* **48** 4087–117
[15] Larson D R *et al* 2003 Water-soluble quantum dots for multiphoton fluorescence imaging *in vivo Sci.* **300** 1434–6
[16] Xu L *et al* 2021 The design strategies and applications for organic multi-branched two-photon absorption chromophores with novel cores and branches: a recent review *J. Mater. Chem. C* **9** 1520–36
[17] Liu H W, Liu Y C, Wang P and Zhang X B 2017 Molecular engineering of two-photon fluorescent probes for bioimaging applications *Methods. Appl. Fluoresc.* **5** 24
[18] Sheppard C J R 2020 Multiphoton microscopy: a personal historical review, with some future predictions *J. Biomed. Opt.* **25** 17

[19] Poudel C and Kaminski C F 2019 Supercontinuum radiation in fluorescence microscopy and biomedical imaging applications *J Opt. Soc. Am. B* **36** A139–53
[20] Hortholary T, Carrion C, Chouzenoux E, Pesquet J C and Lefort C 2021 Multiplex-multiphoton microscopy and computational strategy for biomedical imaging *Microsc. Res. Tech.* **84** 1553–62
[21] Xi P, Andegeko Y, Pestov D, Lovozoy V V and Dantus M 2009 Two-photon imaging using adaptive phase compensated ultrashort laser pulses *J. Biomed. Opt.* **14** 7
[22] Nobis D *et al* 2019 Single-molecule detection of a fluorescent nucleobase analogue via multiphoton excitation *J. Phys. Chem. Lett.* **10** 5008–12
[23] Samaan G N *et al* 2021 Single-molecule fluorescence detection of a tricyclic nucleoside analogue *Chem. Sci.* (https://doi.org/10.1039/D0SC03903A)
[24] Fisher R S *et al* 2018 Pulse-shaped two-photon excitation of a fluorescent base analogue approaches single-molecule sensitivity *Phys. Chem. Chem. Phys.* **20** 28487–98
[25] Lane R S K and Magennis S W 2012 Two-photon excitation of the fluorescent nucleobase analogues 2-AP and tC *RSC Adv.* **2** 11397–403
[26] Masters B R 2010 The origins of Maria Göppert's dissertation on two-photon quantum transitions at Göttingen's Institutes of Physics 1920-1933. *Third international conference on the history of quantum physics; 2010; Berlin* ed S Katzir, C Lehner and J Renn (https://doi.org/10.34663/9783945561225)
[27] Kaiser W and Garrett C G B 1961 Two-photon excitation in CaF2:Eu^{2+} *Phys. Rev. Lett.* **7** 229
[28] Boyd R. W. 2008 *Nonlinear Optics* (San Diego: Academic Press) 3rd edn
[29] Meshulach D and Silberberg Y 1999 Coherent quantum control of multiphoton transitions by shaped ultrashort optical pulses *Phys. Rev. A* **60** 1287–92
[30] Walowicz K A, Pastirk I, Lozovoy V V and Dantus M 2002 Multiphoton intrapulse interference 1: Control of multiphoton processes in condensed phases. *J. Phys. Chem. A.* **106** 9369–73
[31] Diels J-C and Rudolph W 2006 *Ultrashort laser pulse phenomena* (Burlington: Academic Press) 2nd edn
[32] (Ed.) Träger F 2012 *Springer Handbook of Lasers and Optics.* (Berlin Heidelberg: Springer) 2nd edn
[33] Monmayrant A, Weber S and Chatel B 2010 A newcomer's guide to ultrashort pulse shaping and characterization *J. Phys. B* **43** 34
[34] Lozovoy V V, Pastirk I, Walowicz K A and Dantus M 2003 Multiphoton intrapulse interference. II. Control of two- and three-photon laser induced fluorescence with shaped pulses *J. Chem. Phys.* **118** 3187–96
[35] Dela Cruz J M, Pastirk I, Lozovoy V V, Walowicz K A and Dantus M 2004 Multiphoton intrapulse interference 3: Probing microscopic chemical environments *J. Phys. Chem. A* **108** 53–8
[36] Lozovoy V V, Pastirk I and Dantus M 2004 Multiphoton intrapulse interference. IV. Ultrashort laser pulse spectral phase characterization and compensation *Opt. Lett.* **29** 775–7
[37] Comstock M, Lozovoy V V, Pastirk I and Dantus M 2004 Multiphoton intrapulse interference 6; binary phase shaping *Opt. Express* **12** 1061–6
[38] Loriot V, Gitzinger G and Forget N 2013 Self-referenced characterization of femtosecond laser pulses by chirp scan *Opt. Express* **21** 24879–93
[39] Nobis D 2020 Pulse-shaped multiphoton excitation: a new approach to the single-molecule detection of DNA *PhD Thesis* University of Glasgow PhD Thesis
[40] Becker W 2005 *Advanced time-Correlated Single Photon Counting Techniques* (Berlin Heidelberg: Springer)
[41] Becker W 2017 *The bH TCSPC handbook* (Berlin: Becker & Hickl GmbH) 7th edn
[42] Meshulach D and Silberberg Y 1998 Coherent quantum control of two-photon transitions by a femtosecond laser pulse *Nature* **396** 239–42
[43] Ogilvie J P, Debarre D, Solinas X, Martin J L, Beaurepaire E and Joffre M 2006 Use of coherent control for selective two-photon fluorescence microscopy in live organisms *Opt. Express* **14** 759–66
[44] Wilhelmsson L M, Sandin P, Holmen A, Albinsson B, Lincoln P and Norden B 2003 Photophysical characterization of fluorescent DNA base analogue, tC *J. Phys. Chem. B* **107** 9094–101
[45] Sandin P, Wilhelmsson L M, Lincoln P, Powers V E C, Brown T and Albinsson B 2005 Fluorescent properties of DNA base analogue tC upon incorporation into DNA - negligible influence of neighbouring bases on fluorescence quantum yield *Nucleic Acids Res.* **33** 5019–25
[46] Lane R S K, Macpherson A N and Magennis S W 2012 Signal enhancement in multiphoton TIRF microscopy by shaping of broadband femtosecond pulses *Opt. Express* **20** 25948–59
[47] Zhao K, Xu X, Ren W, Jin D and Xi P 2022 Two-photon MINFLUX with doubled localization precision *eLight* **2** 5